Bose-Einstein Condensation of Paraexcitons in Stressed Cu_2O

Jia Ling Lin and J. P. Wolfe

Physics Department and Materials Research Laboratory, University of Illinois at Urbana-Champaign, Urbana, Illinois 61801

(Received 19 March 1993)

Reducing the multiplicity of the orthoexciton ground state in Cu_2O by applying uniaxial stress greatly increases the quantum degeneracy of the excitonic gas produced by intense pulsed excitation. Simultaneously, the paraexciton luminescence spectrum develops an extra component at low energy which is interpreted as a Bose-Einstein condensate of paraexcitons.

PACS numbers: 71.35.+z, 05.30.Jp, 67.90.+z, 78.55.Hx

Since the original experiment by Hulin, Mysyrowicz, and Benoît à la Guillaume [1], who demonstrated Bose-Einstein statistics of orthoexcitons in Cu_2O, concerted attempts have been made to induce Bose-Einstein condensation (BEC) in this nearly ideal-gas system [2,3]. The exciton produced by photoexcitation of a semiconductor is an attractive candidate for BEC due to its small mass as a bound electron-hole pair. Cuprous oxide is particularly suited to this endeavor due to its forbidden direct gap [4], the large excitonic binding energy (150 meV) [4], and the effect of electron-hole exchange to inhibit the formation of complexes such as biexcitons or electron-hole droplets [5].

Because it is composed of an electron and a hole, each with spin $=\frac{1}{2}$, the exciton has both orthoexciton ($S=1$ like) and paraexciton ($S=0$ like) states. The electron-hole exchange interaction produces an ortho-para splitting of 12 meV in Cu_2O, with the paraexciton lying lower [4]. The radiative recombination of orthoexcitons is quadrupole allowed, whereas the paraexciton radiative recombination is forbidden to all orders [6]. When the recombination is assisted by an optical phonon, the paraexciton luminescence becomes weakly allowed [7]. In relatively pure, natural-growth crystals, paraexciton lifetimes of several microseconds have been measured [8]. The orthoexciton lifetime at 2 K is typically 30 ns, due to down conversion to paraexcitons.

The phonon-assisted luminescence spectra directly display the kinetic-energy distributions of the orthoexcitons and paraexcitons. Photoluminescence experiments have shown that, under a wide variety of conditions, the gas of excitons in Cu_2O behaves as an ideal, weakly interacting gas. At low densities a Maxwellian velocity distribution with a temperature near that of the lattice is observed for excitons in pure samples [2,7–9]. To achieve high densities, it is necessary to use pulsed excitation with short-wavelength light, which creates a small effective volume of excitonic gas near the crystal surface. In this case, the gas typically requires a few tens of nanoseconds to relax to the lattice temperature; however, *within a few picoseconds the gas quickly attains an internal temperature T due to frequent collisions between particles* [3].

Time-resolved spectra of orthoexcitons under intense pulsed conditions exhibit Bose-Einstein statistics [2,3,10]. The temperature T and chemical potential μ_i of the ith component of the gas (ortho or para) are directly extracted from the observed spectrum by fitting it to the energy distribution of an ideal Bose gas,

$$N_i(\varepsilon) = D(\varepsilon) f(\varepsilon;\mu_i,T) = C(\varepsilon-\varepsilon_i)^{1/2}/\{\exp[(\varepsilon-\mu_i)/k_BT]-1\}, \quad (1)$$

which assumes the standard Bose-Einstein distribution function $f(\varepsilon;\mu_i,T)$ and the free-particle density of states (per volume), $D(\varepsilon)=C(\varepsilon-\varepsilon_i)^{1/2}$ with $C=g(2/\pi^{1/2})(m/2\pi\hbar^2)^{3/2}$. The energy ε_i marks the band bottom (zero-kinetic-energy level) of the exciton ($i=o$ for ortho and p for para), g is the ground-state multiplicity, and $m=2.7m_e$ for Cu_2O [11]. Given μ_i and T, the density of the ith species of the gas is determined by integrating Eq. (1),

$$n_i = \int_{\varepsilon_i}^{\infty} N_i(\varepsilon)\, d\varepsilon. \quad (2)$$

For pulsed excitation, n_o and T of orthoexcitons evolve in time and a plot of T vs n_o displays a remarkable behavior [2]. Instead of crossing the phase boundary for Bose-Einstein condensation [obtained by setting $\mu_i=\varepsilon_i$ in Eq. (2)],

$$T_c = 0.5273(2\pi\hbar^2/mk_B)(n/g)^{2/3}, \quad (3)$$

the gas temperature is found to closely parallel the phase boundary, maintaining $\mu_o \approx \varepsilon_o - 0.1k_BT$ over a wide range of densities, an effect termed "quantum saturation" [2,10]. The observed heating of the gas is likely to be associated with nonradiative recombination; however, this effect is still not explained in detail.

In the present work we drive the orthoexcitonic gas further towards BEC by reducing the multiplicity factor of the ground state from $g=3$ to $g=1$. This is accomplished by applying a uniaxial stress, σ, along the [110] axis, lowering the symmetry from cubic to orthorhombic [12]. The result is shown in Fig. 1(a). The orthoexciton spectrum, obtained by counting luminescence photons in a 4 ns interval just preceding the peak of a 10 ns Ar-ion laser pulse, is composed of three components whose band-bottom energies (zero kinetic energies) are given by ε_1, ε_2, and ε_3. Because the interconversion of particles between these substates is slower than their lifetimes, each

0031-9007/93/71(8)/1222(4)$06.00

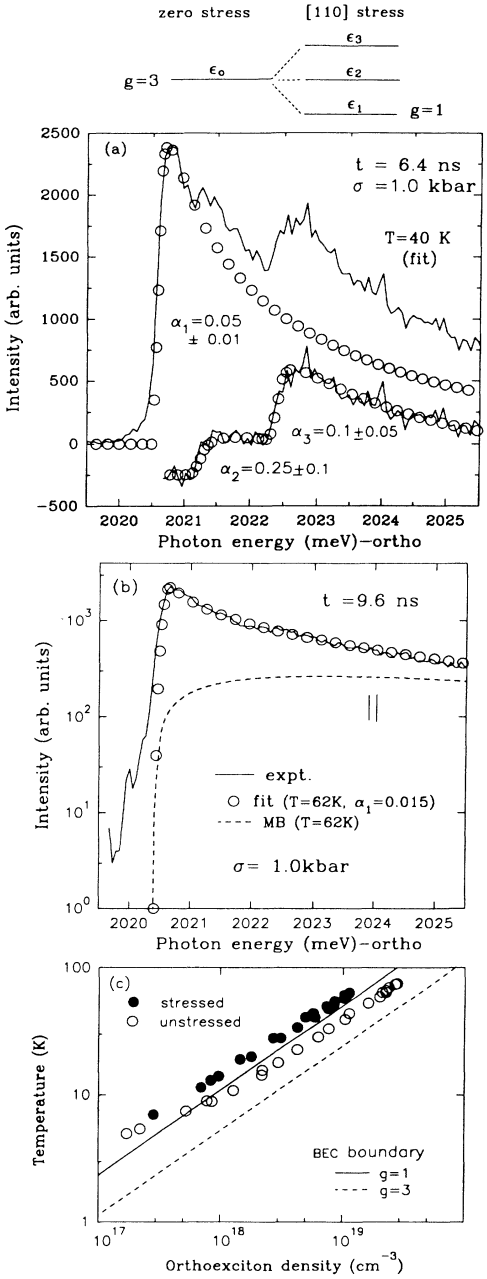

FIG. 1. (a) Time-resolved orthoexciton spectrum showing the three stress-split components. The $1.8\times1.8\times2.8$ mm^3 natural-growth crystal of Cu_2O is immersed in superfluid helium at 1.8 K and excited by 10 ns, 25 W pulses of 514 nm laser light (repetition rate =800 kHz), focused to about 30 μm. The circles represent fits to Eq. (1) with $T=40$ K. The photon energy is related to the exciton energy by the relation $h\nu=\varepsilon-\hbar\Omega$, where $\hbar\Omega$ is the energy of an optical phonon. (b) Orthoexciton spectrum at 45 W peak power, using a polarizer to remove luminescence from the upper stress-split levels. The fit function (circles) is Eq. (1), convolved with the spectral resolution shown. For comparison, a Maxwell-Boltzmann distribution with the same T is plotted as the dashed curve. (c) Quantum saturation effect for the stressed and unstressed cases. The straight lines are the respective phase boundaries for BEC.

species has a distinct chemical potential, μ_i. We assume, however, that the rapid collisions create a single gas temperature, T. It is useful to define a dimensionless measure of the chemical potentials, given by $\alpha_i=(\varepsilon_i-\mu_i)/k_BT$.

The intensities of the upper two levels can be greatly diminished by inserting a linear polarizer with orientation along the stress axis. The remaining ground-level spectrum (not shown) is then fit to Eq. (1), yielding the Bose-Einstein distribution indicated by the open circles on the upper trace. The spectra of the upper two states are isolated by subtracting this spectrum (open circles) from the experimental spectrum obtained without the polarizer (upper trace) and are plotted at the bottom of the figure. The spectra are each fit to Eq. (1), and, as expected, it is found that the three μ_i are not equal at this early sampling time.

The beneficial effect of the reduced multiplicity of the ground state is seen in Fig. 1(b), which is a raw spectrum at somewhat later sampling time, when the population of the upper two levels is reduced. Residual luminescence from the upper levels is removed with a polarizer. The logarithmically displayed fit to a Bose-Einstein distribution is exceptionally good, yielding $T=62$ K and $\alpha_1=0.015$, which is nearly an order of magnitude smaller than that observed in the unstressed crystal and very close to $\alpha_1=0$ for BEC. The $T(n_o)$ evolution of the orthoexciton gas in the stressed crystal is obtained by similarly analyzing spectra at other times and using Eq. (2) to determine n_o. The data are compared to the previously published data for the unstressed case [2] in Fig. 1(c). With stress, the orthoexciton gas displays a quantum saturation which is much closer to the BEC phase boundary [Eq. (3) with $g=1$] than for the unstressed crystal ($g=3$); *however, no evidence for a condensed phase is seen in the orthoexciton* spectra.

We now examine the much weaker luminescence from the paraexcitons. As shown in Fig. 2(a), the paraexciton spectrum (heavy curve) is significantly narrower than that of the orthoexcitons (dashed curve, shifted by 8.4 meV). In fact, it is impossible to fit the paraexciton spectrum solely with Eq. (1), even assuming $\alpha_p=0$. An $\alpha_p=0$ spectrum, using the measured temperature of the orthoexciton gas and the experimental spectral resolution, is plotted as the solid dots in the figure. We have chosen an amplitude to match the high-energy edge of the paraexciton spectrum. Clearly there is a significant amount of intensity at low energies which is not accounted for by the "excited-state distribution," $N_p(\varepsilon)$. At earlier sampling times, significant amount of luminescence from a nearby orthoexciton phonon-replica obscures the high energy side of the paraexciton spectrum. [A small contribution from this source can be seen above 2013.5 meV in Fig. 2(a).]

The extra luminescence component required to explain the paraexciton spectrum is slightly broader than our spectral resolution. A Gaussian line with full width at

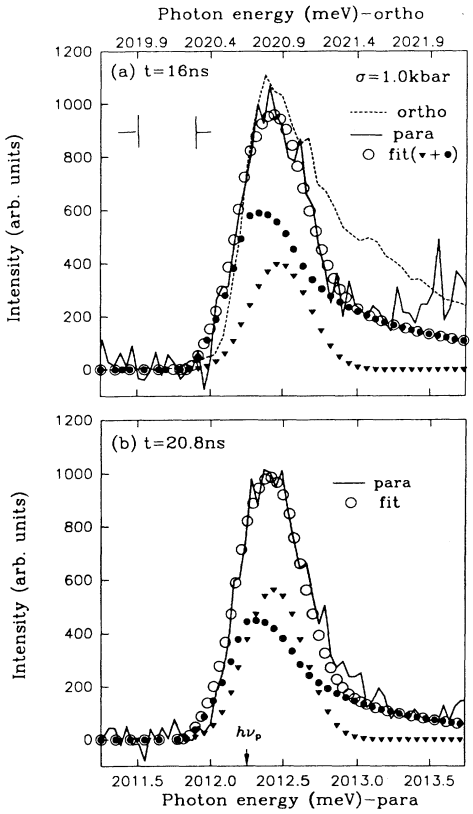

FIG. 2. (a) The dark curve is the paraexciton luminescence in the stressed crystal, obtained under the same conditions as Fig. 1(b). The dashed curve is the orthoexciton luminescence recorded at much lower gain for the same delay time and a spectral resolution of 0.14 meV. Solid dots are a slit-broadened Bose-Einstein distribution, $N_p(\varepsilon)$, with $\alpha_p=0$ and $T=14$ K extracted from the ortho spectrum. Triangles define a Gaussian line of full width at half maximum 0.5 meV convolved with the spectral resolution shown, 0.41 meV. The sum of Gaussian and excited-state $[N_p(\varepsilon)]$ components, convolved with slit function, is given by the circles. (b) Paraexciton spectrum at a later sampling time, showing a larger low-energy component (triangles) and an excited-state component (dots) with $T=9.5$ K from the ortho fit (not shown).

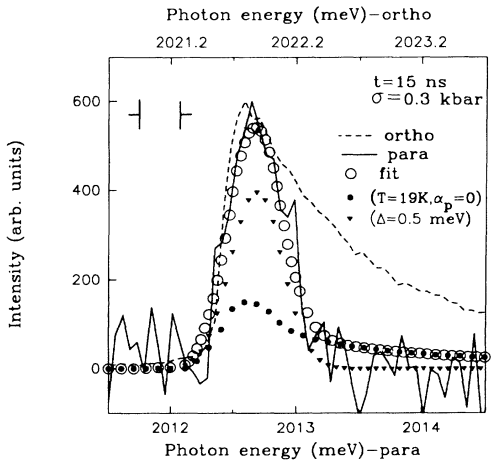

FIG. 3. Paraexciton spectrum obtained at somewhat lower stress and higher power than in Fig. 2. The spectral resolution is 0.33 meV. A polarizer eliminates the nearby orthoexciton phonon replica. There remains a slight base line shift across this weak paraexciton spectrum. The superimposed orthoexciton spectrum is taken with a spectral resolution of 0.14 meV and its peak is normalized to that of the paraexciton.

half maximum (FWHM) equal to 0.5 ± 0.02 meV convolved with our triangular "slit function" (FWHM $=0.41$ meV) and centered at $h\nu=2012.4$ meV represents the extra luminescence quite well. This new component is "blueshifted" about 0.2 meV ($=2.4$ K) above $h\nu_p=\varepsilon_p-\hbar\Omega_{\text{phonon}}=2012.2$ meV, which corresponds to the zero in kinetic energy for paraexcitons at low gas density. A component with the same spectral position and width also accounts for the extra luminescence in the later spectrum shown in Fig. 2(b). In this case, the intensity of the low-energy component is larger than the excited-state component, $N_p(\varepsilon)$.

The relative amount of low-energy and excited-state components depends upon experimental conditions. A striking spectrum obtained at somewhat different stress and excitation conditions is plotted in Fig. 3. The spectrum consists nearly entirely of the low-energy component (with a blueshift of 0.2 meV), whereas the orthoexciton spectrum (dashed curve) displays a broader, excited-state distribution.

What is the gas density of the paraexcitons? It can be estimated from their luminescence intensity relative to that of the orthoexcitons. The orthoexciton densities are obtained from Eq. (2) using the spectrally determined α_1 and T. In Fig. 4(a) we plot the spectrally integrated intensities of the ortho- and paraexciton luminescence lines. The paraexciton intensity is multiplied by a factor of 500—the ratio of radiative efficiencies of the two species [7]—so the ratio of gas densities for the two species can be determined from the graph [13]. We see that the ortho- and paraexciton densities follow each other closely at early times, but beyond the peak of the laser pulse, the paraexciton density continues to increase while the orthoexciton density decreases, consistent with its shorter lifetime.

In Fig. 4(b) we plot the observed $T(n)$ relations for both orthoexcitons and paraexcitons. With stress the BEC phase boundary is the same for both species ($g=1$). The orthoexcitons quantum saturate at $\alpha_1\approx0.04$. *The paraexcitons cross the phase boundary for Bose-Einstein condensation*, coincident with the appearance of the low-energy spectral component. We conclude that the new spectral component represents the condensate. The solid dots in Fig. 3 give the $\alpha_p=0$ excited-state spectrum with a relative intensity derived from Fig. 4. In both Figs. 2 and 3, good fits to the spectra are also obtained when the condensate and excited-state components are assumed to have the same blueshift of about 0.2 meV.

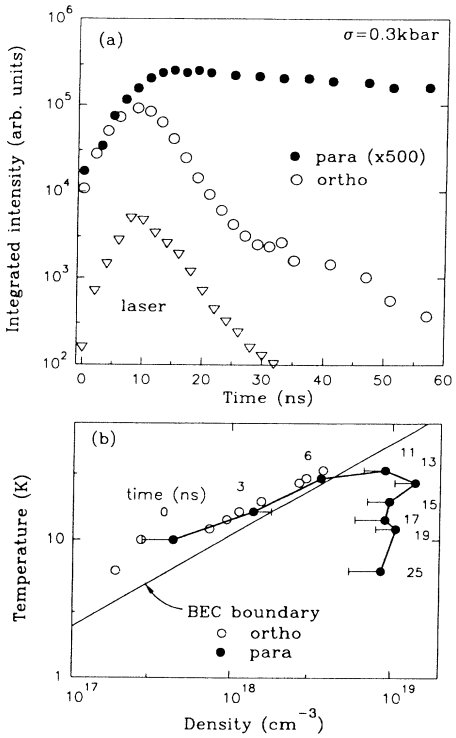

FIG. 4. (a) Spectrally integrated intensities of the ortho and para luminescence as a function of time. Multiplying the para signal by 500 indicates the relative densities of the two species at early times, assuming that they occupy the same volume. Triangles give the laser profile. (b) Plots of $T(n)$ for the ortho- and paraexciton gases. Sampling times are indicated for each of the ortho-para data pairs. The paraexciton density crosses into the BEC region at about 11 ns.

The blueshift of the condensed gas could have several explanations. In a nearly free Bose gas [14], repulsive interactions between particles lead to an energy renormalization of $\Delta\varepsilon = 2\pi\hbar^2 na/m$. Assuming $\Delta\varepsilon = 0.2$ meV, this relation implies a "hard core" diameter of the excitons given by $a = 2$ Å, somewhat smaller than the Bohr radius of 7 Å. Alternatively, the shift of 0.2 meV corresponds to a drift velocity of 5×10^5 cm/s for the condensate, about that of the longitudinal phonons in Cu_2O [15].

Why is the application of stress favorable to the *paraexciton* condensation? Several factors come to mind, which must be tested in later work. First, due to the reduced g for orthoexcitons, the overall quantum degeneracy of the two-component gas is higher, helping to initiate BEC. Second, the reduced symmetry may increase the rate of ortho-to-para conversion. Third, the coupling of the paraexcitons to transverse acoustic phonons becomes nonzero in the stressed case [9]. A corresponding reduction in the diffusivity of the excitonic gas would decrease the effective volume and thereby increase the gas density. Also, an increase in the electron-phonon coupling should improve the cooling of the gas.

The quantitative and qualitative conclusions of this work are based upon the collective knowledge gained by previous time- and space-resolved studies in unstressed Cu_2O. In particular, we have assumed in our present analyses that the interpenetrating ortho- and paraexciton gases have the same temperature and occupy essentially the same volume over the measurement period. We presently have no reason to doubt that these properties continue to be valid in the stressed case.

We are grateful to D. Snoke, A. Mysyrowicz, and D. Trauernicht for valuable contributions leading to the present work. G. Baym has provided critical ideas in the interpretation of our data. The crystal was kindly supplied by P. J. Dunn of the Smithsonian Institute. This work is supported by the National Science Foundation under Grant No. NSF DMR 92-07458.

[1] D. Hulin, A. Mysyrowicz, and C. Benoît à la Guillaume, Phys. Rev. Lett. **45**, 1970 (1980).
[2] D. Snoke, J. P. Wolfe, and A. Mysyrowicz, Phys. Rev. Lett. **59**, 827 (1987).
[3] D. W. Snoke and J. P. Wolfe, Phys. Rev. B **42**, 7876 (1990), and references therein.
[4] For a review of Cu_2O properties see V. T. Agekyan, Phys. Status Solidi A **43**, 11 (1977).
[5] F. Bassani and M. Rovere, Solid State Commun. **19**, 887 (1976); A. I. Bobrysheva and S. A. Moskalenko, Phys. Status Solidi B **119**, 141 (1983).
[6] P. D. Bloch and C. Schwab, Phys. Rev. Lett. **41**, 514 (1978).
[7] See Ref. 10 in D. W. Snoke, Jia Ling Lin, and J. P. Wolfe, Phys. Rev. B **43**, 1226 (1991).
[8] A. Mysyrowicz, D. Hulin, and A. Antonetti, Phys. Rev. Lett. **43**, 1123 (1979); **43**, 1275E (1979).
[9] D. P. Trauernicht and J. P. Wolfe, Phys. Rev. B **33**, 8506 (1986).
[10] D. W. Snoke, J. P. Wolfe, and A. Mysyrowicz, Phys. Rev. Lett. **64**, 2543 (1990); Phys. Rev. B **41**, 11171 (1990).
[11] N. Caswell, J. S. Weiner, and P. Y. Yu, Solid State Commun. **40**, 843 (1981).
[12] R. J. Elliot, Phys. Rev. **124**, 340 (1961); R. G. Waters, F. H. Pollak, R. H. Bruce, and H. Z. Cummins, Phys. Rev. B **21**, 1665 (1980), and references therein.
[13] We believe that for these phonon-assisted replicas this ratio is not significantly modified by the stress. See Agekyan, Ref. [4].
[14] The effect of interactions in the quantum gas have been considered by Yu. M. Kagan, B. V. Svistunov, and G. V. Shlyapnikov, Zh. Eksp. Teor. Fiz. **101**, 528 (1992) [Sov Phys. JETP **74**, 279 (1992)]; S. A. Moskalenko, A. I. Bobrysheva, S. S. Russu, V. V. Balgata, and A. V. Lelyakov, J. Phys. C **18**, 989 (1985).
[15] Rapid expansion of the quantum-degenerate gas has been observed in Refs. [2] and [10]. Explanations of this behavior have been forwarded by Bennett Link and Gordon Baym, Phys. Rev. Lett. **69**, 2959 (1992); A. E. Bulatov and S. G. Tikhodeev, Phys. Rev. B **46**, 15058 (1992).